



# Road-blocker HSP disease mutation disrupts pre-organization for ATP hydrolysis in kinesin through a second sphere control

Rabindra Nath Manna<sup>a</sup> , José N. Onuchic<sup>b,c,d,e,1</sup> , and Biman Jana<sup>a,1</sup>

Contributed by José N. Onuchic; received September 7, 2022; accepted November 16, 2022; reviewed by Shoji Takada and Dave Thirumalai

Kinesin motor proteins perform several essential cellular functions powered by the adenosine triphosphate (ATP) hydrolysis reaction. Several single-point mutations in the kinesin motor protein KIF5A have been implicated to hereditary spastic paraplegia disease (HSP), a lethal neurodegenerative disease in humans. In earlier studies, we have shown that a series of HSP-related mutations can impair the kinesin's long-distance displacement or processivity by modulating the order–disorder transition of the linker connecting the heads to the coiled coil. On the other hand, the reduction of kinesin's ATP hydrolysis reaction rate by a distal asparagine-to-serine mutation is also known to cause HSP disease. However, the molecular mechanism of the ATP hydrolysis reaction in kinesin by this distal mutation is still not fully understood. Using classical molecular dynamics simulations combined with quantum mechanics/molecular mechanics calculations, the pre-organization geometry required for optimal hydrolysis in kinesin motor bound to  $\alpha/\beta$ -tubulin is determined. This optimal geometry has only a single salt-bridge (of the possible two) between Arg203-Glu236, putting a reactive water molecule at a perfect position for hydrolysis. Such geometry is also needed to create the appropriate configuration for proton translocation during ATP hydrolysis. The distal asparagine-to-serine mutation is found to disrupt this optimal geometry. Therefore, the current study along with our previous one demonstrates how two different effects on kinesin dynamics (processivity and ATP hydrolysis), caused by a different set of genotypes, can give rise to the same phenotype leading to HSP disease.

Kinesin motor protein | ATP hydrolysis mechanism | HSP disease | classical MD simulations | QM/MM calculations

Kinesin-1 is a motor protein that walks along microtubule (MT) filaments toward the plus-ends using energy acquired from the adenosine triphosphate (ATP) hydrolysis reaction while performing various cellular activities. For instance, it is responsible for the intracellular transport of vesicles, organelles, and signaling complexes (1–3). Neuronal kinesin KIF5A, for example (4, 5), is particularly important for retrograde axonal transport inside neurons. Several single-point mutations of the KIF5A kinesin are found to be extremely pathological, leading to a lethal neurodegenerative disease in humans, hereditary spastic paraplegia (HSP) disease (6, 7).

Generally, kinesin motor proteins function in a homodimeric state. In earlier studies (8, 9), we have shown that all kinesins have some structurally important regions: motor domains which perform the catalytic conversion of ATP as well as binding to the MT, the coiled-coil stalk region that is essential for dimerization, and the neck linker region that connects the motor domain to the coiled-coil stalk region. It was shown that the energetic balance between kinesin binding to the MT and coiled-coil interactions in the dimerization interface is crucially important for the required order–disorder transition of the neck linker (8). This transition mediates the coordination between two motor domains of the kinesin dimer faithfully, which is required for a long-distance run on the MT. This process is referred to as processivity (10, 11). On the other hand, the rate of hydrolysis of ATP determines the gliding velocity of the kinesin on the MT. It is important to note here that the processivity, directionality of stepping, and gliding velocity are crucial for their function (7–12).

Mutations related to HSP disease are genotypic. While most of these mutations are found to be in the motor domain of the kinesin, some are also found to be in the dimerization region. As shown in our earlier studies, which investigated the effect of HSP disease-related mutations on the dynamics of kinesin, these mutations are either at the MT-binding interface or at the dimerization region. Therefore, they destroy the energetic balance between the relative strength of these interactions, impairing the kinesin processivity that leads to HSP disease (8, 9). However, some other mutations in the motor domain are found not to affect the MT-binding strength but also lead to the disease. Experiments have shown that those mutations actually reduce the rate of ATP hydrolysis

## Significance

Kinesin, an amazing biological machine, converts chemical energy from the ATP hydrolysis into mechanical energy to perform different cellular activities. Several single-point gene-level mutations in the neuronal kinesin motor (KIF5A) are linked to a neurodegenerative disease, hereditary spastic paraplegia (HSP). Earlier we demonstrated that some of the mutations produce inefficient kinesins that can only walk a few steps on a microtubule as opposed to several hundred by normal kinesin. Here, a different mutation is studied that produces very sluggish kinesin by reducing the rate of hydrolysis of ATP. This asparagine-to-serine mutation at distal location to the active site is shown to disrupt pre-organization environment required for efficient ATP hydrolysis reaction in kinesin through a second sphere effect.

Author contributions: R.N.M., J.N.O., and B.J. designed research; R.N.M. performed research; R.N.M., J.N.O., and B.J. analyzed data; and R.N.M., J.N.O., and B.J. wrote the paper.

Reviewers: S.T., Kyoto Daigaku; and D.T., The University of Texas at Austin.

The authors declare no competing interest.

Copyright © 2022 the Author(s). Published by PNAS. This article is distributed under [Creative Commons Attribution-NonCommercial-NoDerivatives License 4.0 \(CC BY-NC-ND\)](https://creativecommons.org/licenses/by-nc-nd/4.0/).

<sup>1</sup>To whom correspondence may be addressed. Email: jonuchic@rice.edu or pcbj@iacs.res.in.

This article contains supporting information online at <https://www.pnas.org/lookup/suppl/doi:10.1073/pnas.2215170120/-/DCSupplemental>.

Published December 27, 2022.

and thereby affect the gliding velocity of the kinesin (6, 7). It has been proposed that such kinesins, due to their sluggish movement, act as road blockers for other normally moving kinesin. In this article, we will concentrate on one of such mutations which is distal to the ATP hydrolysis reaction center.

Like other motor proteins (13–25), the hydrolysis of the ATP molecule is an essential step in the mechanochemical cycle of kinesin. Here we focus on the mutation of the asparagine residue at a distal position with respect to the hydrolysis reaction center that is changed to a serine residue (Asn255Ser for PDB ID: 4HNA) (26). This mutation causes a reduction in the kinesin gliding velocity on the MT and in the ATPase rate compared to the wild-type one (8). The large distance (~11.5 Å) between the asparagine residue and the terminal  $\gamma$ -phosphorus atom of the ATP in the kinesin-1 structure suggests a long-distance or second sphere control of the ATP hydrolysis reaction (Fig. 1). Similar large distance effects have been previously observed. Biochemical studies have shown that the rate of ATP hydrolysis of kinesin-1 increases by ~33-fold upon binding to the MT (6). The MT-binding site and ATP hydrolysis reaction center are also far apart from each other (Fig. 1). Herein, using all-atom explicit solvent molecular dynamics (MD) simulations, hybrid quantum mechanics/molecular mechanics (QM/MM) methods, and an enhanced sampling approach for calculating free energies, we provide an explanation for the molecular origin of this second sphere control of the ATP hydrolysis reaction in kinesin-1, which is

needed to understand its connection to HSP disease. In this connection, it is important to note that an earlier study (23) on this topic focusing on the ATP hydrolysis mechanism of kinesin did not consider the effect of MT binding and was limited to aqueous kinesin only. Inclusion of the MT-bound state is required to understand the complete process of ATP hydrolysis which is attempted in this study.

In this study, we will first present the three different reaction schemes for the ATP hydrolysis reaction in the wild-type kinesin bound to MT. We will then discuss our findings on the reaction mechanism and energetics for those three reaction schemes using hybrid QM/MM calculations and most importantly determine the pre-organization geometry for the reaction. Next, the effect of mutation and MT unbinding on the pre-organization geometry will be described using all-atom explicit solvent MD simulations and an enhanced sampling approach for calculating free energies. A multiple sequence alignment will also be presented to show how important are the residues/interactions of pre-organization geometry. Finally, we will discuss our results in the context of the HSP disease.

## Results and Discussion

**Probing ATP Hydrolysis Reaction Mechanism to Extract Pre-Organization Geometry.** Standard MD simulation of the MT-bound kinesin-1 with ATP in its active site provides the equilibrium geometry of the reaction center (Fig. 1). A  $Mg^{2+}$  ion forms an octahedral coordination with two water molecules, two hydroxyl groups from Thr92 and Ser202 residues, and two non-bridged oxygen atoms of the ATP molecule (*SI Appendix, Fig. S1*). A salt-bridge pair between the Arg203 and Glu236 residues is found to be in close proximity to the ATP molecule. Additionally, a few other water molecules were present near and around the reaction center. On the basis of classical dynamics, three distinctly different reaction schemes for the ATP hydrolysis process in the kinesin- $\alpha/\beta$ -tubulin complex are proposed in order to better understand the role of active site residues and water molecules (Fig. 2). In model A, a lytic water molecule attacks the terminal phosphorus atom of the ATP substrate and the same water molecule also provides the proton to complete the reaction. Within model B, three water molecules are directly and cooperatively engaged in the hydrolysis reaction. One water molecule acts as attacking water, one as proton donor while the other one acts as mediator for proton transfer. In model C, the Arg203-Glu236 salt-bridge is broken and phosphate hydrolysis reaction occurs in a stepwise manner. Here, Glu236 acts as a base to activate the lytic water molecule triggered by the relay proton transfer mechanism via a second water molecule in the first step. The proton ended up on Glu236, and yielding  $HPO_4^{2-}$  as an intermediate product. In the subsequent step, one of the oxygen atoms of the  $HPO_4^{2-}$  abstracts a proton from another water molecule, Glu236 is deprotonated via a relay proton shuttle, and the final product is formed. Next, QM/MM simulations of three different reaction models were performed for the ATP hydrolysis reaction in the MT-bound kinesin-1. These simulations provide the possible mechanisms and pre-organization geometries required for optimal hydrolysis (Fig. 2). Several configurations of the ATP-bound kinesin-MT complex are selected from our classical MD simulations based on different choices for the water chain between the ATP and the Arg203-Glu236 salt-bridge and for the orientation/stabilities of the Arg203-Glu236 salt-bridge pair. These configurations are used as initial structures for our (QM/MM) optimization calculations. Over the last decades, unrevealing the mechanism of the ATP hydrolysis reactions has come into prominence for ATP-dependent molecular motor proteins, such as kinesin, myosin, dynein, F1-ATPase, and

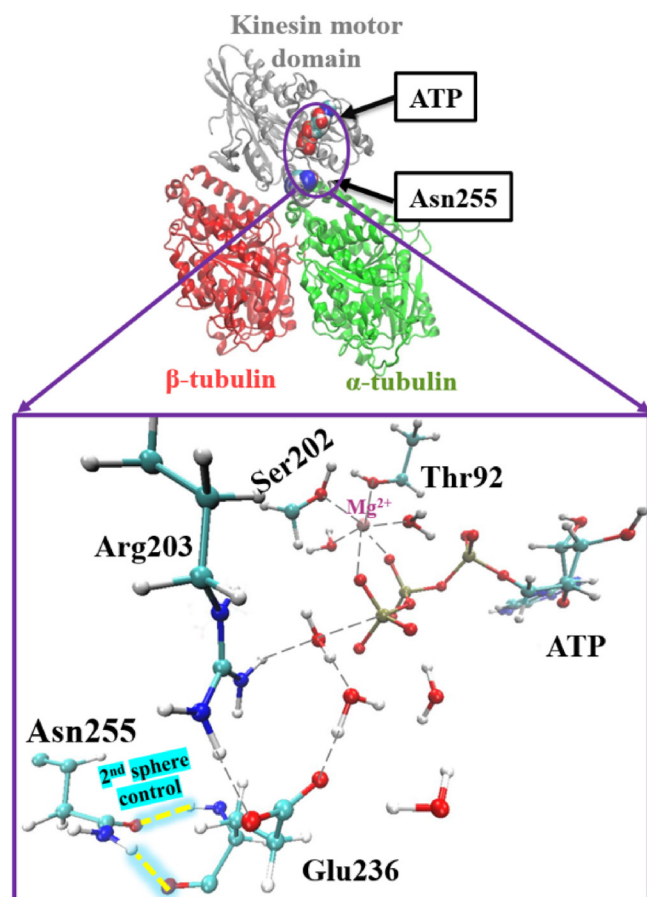


**Fig. 1.** ATP-bound kinesin- $\alpha/\beta$ -tubulin complex. It is composed of the kinesin motor domain region,  $\alpha$ -tubulin, and  $\beta$ -tubulin. The tubulins are the units of the microtubule filaments. The  $\gamma$ -phosphate group of the ATP is surrounded by the Glu236, Arg203, Ser202, Thr92,  $Mg^{2+}$  ion, and six water molecules. The HSP disease-related residue, Asn255, is also shown, and the proposed second sphere interactions are highlighted.

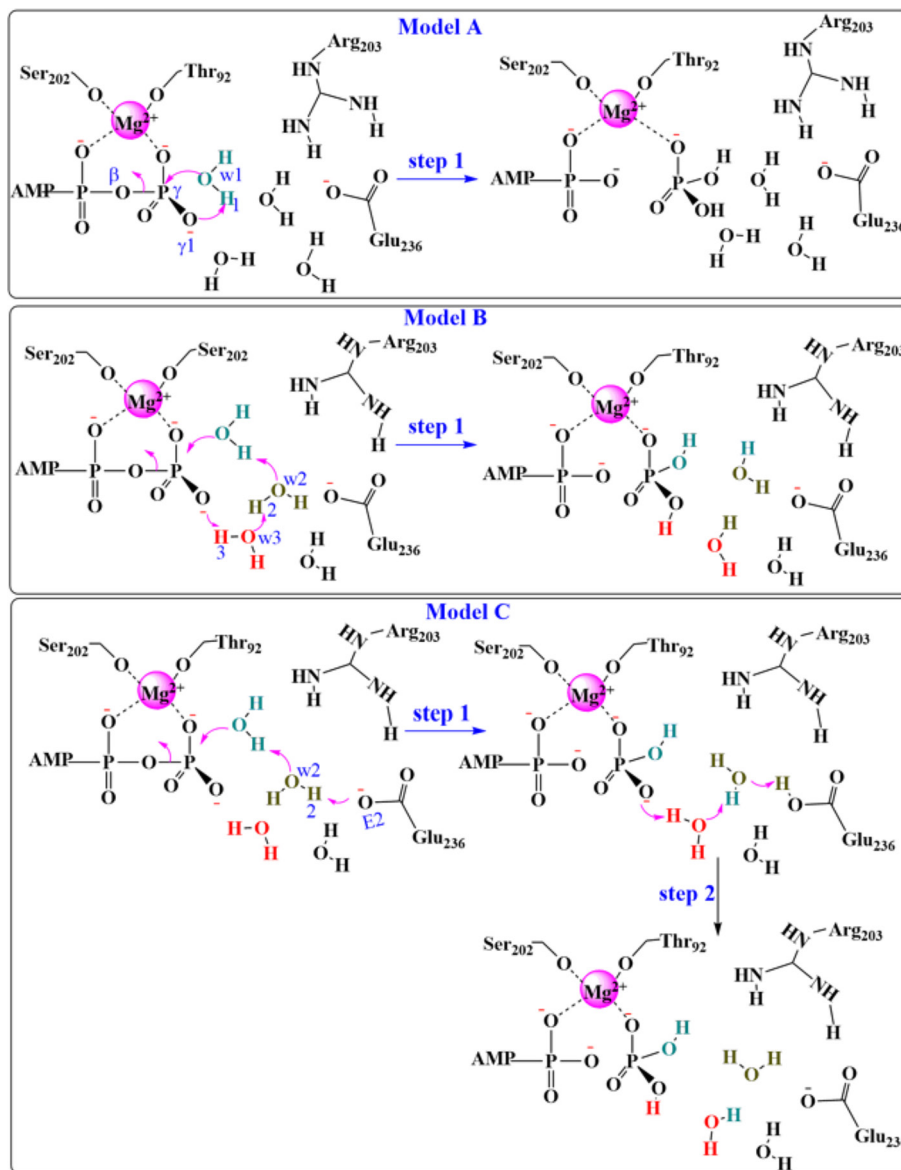


**Fig. 2.** The proposed mechanisms for the ATP hydrolysis reaction in the kinesin- $\alpha/\beta$ -tubulin complex. AMP denotes adenosine monophosphate. To simplify, the coordination of  $Mg^{2+}$  ion with two water molecules is not shown. Displayed atom numbering and nomenclature are used throughout this study. In model A, a lytic water ( $w1$ ) molecule attacks the terminal phosphorus atom ( $P_{\gamma}$ ) of the ATP substrate of the kinesin-tubulin complex and a proton ( $H1$ ) from the lytic water ( $w1$ ) is shifted to the  $\gamma$ -phosphate group to yield an inorganic phosphate ( $H_2PO_4^-$ ). The salt-bridge pair of Arg203-Glu236 remains fully intact during this process. In model B, Arg203-Glu236 salt-bridge pair is transiently broken. The OE2 atom of the carboxylic group of the Glu236 residue establishes a strong hydrogen bond with the second water molecule during the hydrolysis reaction. Simultaneously, a proton transferred from the lytic water molecule to one of the non-bridge oxygen atom ( $O_{\gamma 1}$ ) of the terminal  $\gamma$ -phosphate of the ATP to form an inorganic phosphate through the proton translocation mechanisms. Within model C, phosphate hydrolysis reaction occurs in a stepwise manner. The Glu236 activates the lytic water molecule through the relay proton transfer mechanism via the second water molecule. Glu236 acts as a base, the proton ended up on Glu236, and yielding  $HPO_4^{2-}$  as a product. In the second step, one of the oxygen atoms of the  $HPO_4^{2-}$  abstracts a proton from the third water, and consequently, Glu236 is un-protonated via relay proton shuttle from the Glu236 to the third water.

GTPases (13–25). These studies reinforce a common mechanism involving a proton transfer mechanism with the help of either an active site residue (such as Glu, Asp, Lys), an Arg-Glu salt-bridge pair, or neighboring water molecules. In our QM/MM model A, a lytic water ( $w1$ ) attacks the  $P_{\gamma}$  atom of the ATP, and subsequently, the same water is deprotonated to form the inorganic phosphate ( $H_2PO_4^-$ ) and ADP (*SI Appendix, Fig. S2*). The activation barrier for the ATP hydrolysis reaction of model A is 39.4 kcal/mol when computed using a B3LYP-D3/def2-TZVP/OPLS level of theory (Fig. 3). To decipher whether the proton translocation happens directly from an attacking water or via a neighboring auxiliary one, we have explored another model (i.e., model B) in which three water molecules are explicitly involved in the reaction mechanism.

Here, a second water molecule ( $w2$ ) concurrently acts as a base and a proton transporter. It abstracts a proton from the lytic water ( $w1$ ) molecule, the  $P_{\gamma}$ - $O_{w1}$  bond is formed, and a relay proton transfer happens, all the way, from the lytic water molecule to the non-bridged  $O_{\gamma 1}$  atom of the  $\gamma$ -phosphate of the ATP molecule through another auxiliary water molecule ( $w3$ ) (see *SI Appendix, Fig. S3* for details). The second water molecule is stabilized by Glu236 through a hydrogen-bonding interaction. Our results show indeed multiple water molecules mediating ATP hydrolysis reaction. In this case, the activation barrier is 19.7 kcal/mol, and therefore, the reaction is significantly more feasible than model A.

In model C, a broken salt-bridge Arg203-Glu236 of the enzyme-substrate state activates the lytic water ( $w1$ ) through a

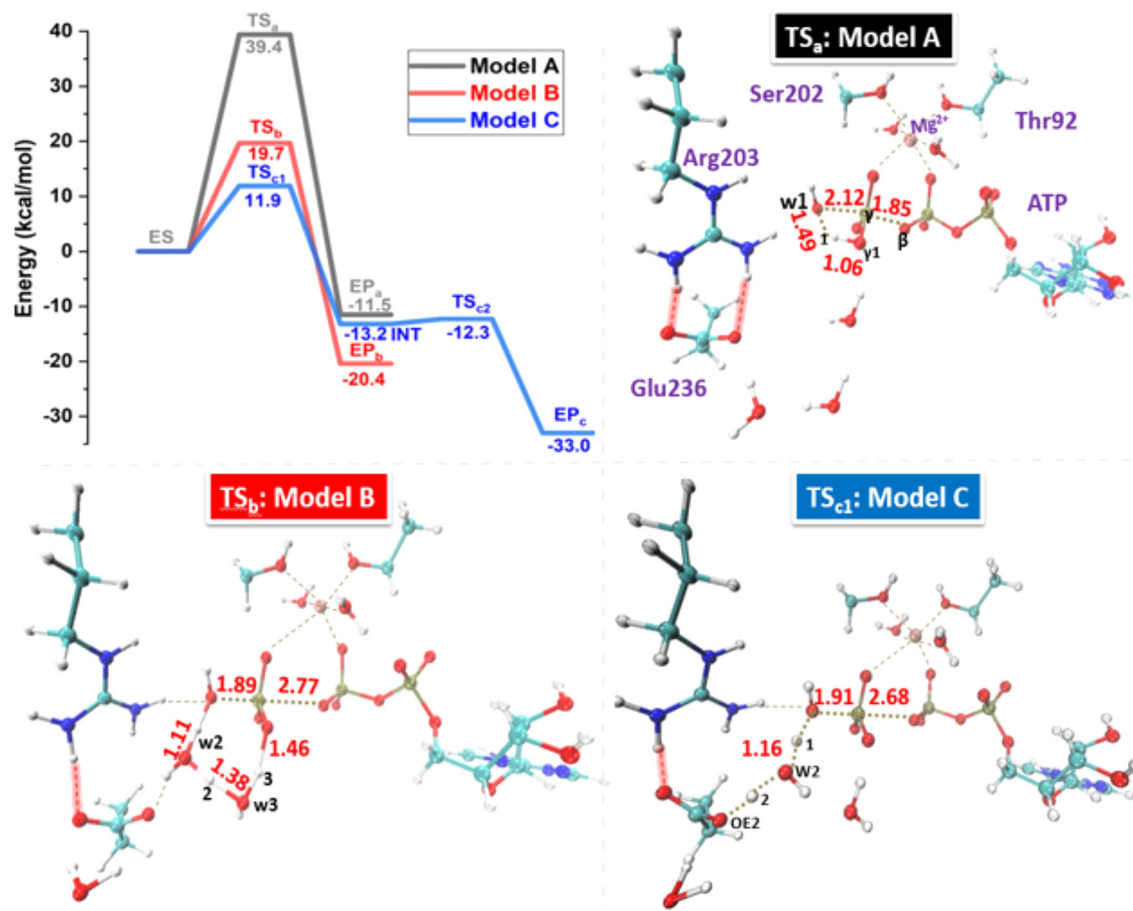


**Fig. 3.** Potential energy profiles of the ATP hydrolysis reaction of the kinesin- $\alpha/\beta$ -tubulin complex for the different reaction schemes at the B3LYP-D3/def2-TZVP/OPLS level of theory. QM/MM optimization calculations were first performed at the B3LYP/6-31+G(d,p)/OPLS level of theory. Subsequently, the energies of all the optimized stationary state structures were corrected by single-point calculations using dispersion-included B3LYP-D3/def2-TZVP/OPLS level of theory.  $TS_a$  and  $TS_b$  represent the transition states along the path for models A and B, respectively.  $TS_{c1}$  and  $TS_{c2}$  represent the transition state structures along the path for model C. Furthermore, ES, INT, and EP denote enzyme-substrate complex, intermediate, and enzyme-product complex, respectively. Optimized  $TS_a$ ,  $TS_b$ , and  $TS_{c1}$  structures with the key interatomic distances (Å) are presented.

relay proton translocation mechanism with the participation of auxiliary water molecules. The Glu236-assisted ATP hydrolysis reaction is divided into two steps (*SI Appendix, Fig. S4*). In the first step, Glu236 abstracts a proton from the second water (w2) which helps to activate the lytic water (w1) through the relay proton transfer mechanism with an extended network engaging the ATP, lytic water, second water, and Glu236. In this step, the phosphate hydrolysis is started by the cleavage of the  $P_\gamma$ - $O_\beta$  bond ( $TS_{c1}$ : 2.68 Å) and concurrently the  $P_\gamma$ - $O_{w1}$  bond is formed ( $TS_{c1}$ : 1.91 Å) (Fig. 3). The activation energy barrier for the  $\gamma$ -phosphate hydrolysis process of the ATP is 11.9 kcal/mol, and the associated stability of the intermediate is exothermic by -13.2 kcal/mol. In the second step, a proton from the carboxylic moiety of the Glu236 is transferred to the  $O_{\gamma 1}$  atom of the ATP through another proton transfer mechanism involving another auxiliary water molecule (w3) to form an inorganic moiety ( $H_2PO_4^-$ ). This process has a low barrier (0.9 kcal/mol) associated to an exothermic process with an overall reaction energy of -33.0 kcal/mol. Here, Glu236 is acting as a base as well as a proton reservoir during the ATP hydrolysis reaction. MOFJ analysis showed that ATP hydrolysis in kinesin follows a so-called concerted-like pathway in its rate-limiting step (*SI Appendix, Fig. S5*). Our computed barrier for the ATP hydrolysis reaction of this model system is in a comparable range with the experimental barrier (12.4 kcal/mol) as derived from its rate constant ( $k_{cat}$ :  $17.58 \text{ s}^{-1}$ ) (7). The  $Mg^{2+}$  ion

plays an important role to stabilize the enzyme-substrate, the transition state (TS), and the enzyme-product state structures by forming an octahedral coordination sphere with two non-bridging oxygen atoms of the ATP, two water molecules, and the Ser202 and Thr92 residues, respectively (*SI Appendix, Tables S2–S4*). It is noteworthy to mention that the Arg203-Glu236 salt-bridge pair remains intact in model A (high barrier) and is broken for both models B and C (low barrier). In particular, for model C, the broken salt-bridge is an absolute necessity for the proper pre-organization geometry of the reaction. Our findings spell out that model C is most favorable pathway for ATP hydrolysis reaction. Therefore, model C provides optimal pre-organization environment for efficient ATP hydrolysis reaction in this system. The broken salt-bridge-assisted water-mediated mechanistic pathway for the ATP hydrolysis process (model C) in kinesin was also suggested in a previous study by McGrath et al. (23) The broken configuration of the salt-bridge ensures the lytic water (w1) position by a hydrogen-bonding interaction with Arg203 and the proton abstraction from auxiliary water (w2) by Glu236, needed for initiating the activation of lytic water through proton translocation. The mechanistic picture emerging from our extensive calculations implied that the water molecules present close to the kinesin motor protein's active site play a key role in the binding of the ATP substrate, the subsequent ATP hydrolysis reaction, and the release of the product. Our study along with several others

revealed that one of the vital aspects in an enzymatic ATP/GTP hydrolysis reaction is a relay proton transfer event through an extended water chain during different steps of the reaction, suggesting a common mechanism (13–22).

**Effect of Disease-Related Mutation and MT Binding on the Pre-Organization Environment.** Next, to explore the effect of binding to the MT and the Asn255Ser mutation on this pre-organization, we have performed MD simulations of the ATP-bound wild-type kinesin (W), of the wild-type kinesin- $\alpha/\beta$ -tubulin (W-MT), and of the mutated (Asn255Ser) kinesin- $\alpha/\beta$ -tubulin (M-MT) complexes. First, we examined the stability of the salt-bridge pair between Arg203 and Glu236 residues. In an earlier study, McGrath et al. suggested the involvement of the Arg203-Glu236 salt-bridge pair during the ATP hydrolysis for the wild-type kinesin (23). These studies, however, have not quantified the stability and the orientation of this salt-bridge. Herein, the minimum interatomic distances of NH1-OE1 (or OE2) and NH2-OE1 (or OE2) have been computed for the last 50 ns of the equilibrium MD simulations of the three systems (Fig. 4). For the W-MT system, the minimum distance of NH1-OE1 (or OE2) remains well below 3.5 Å throughout the MD simulations, whereas the minimum distance of NH2-OE2 (or OE1) fluctuates in the range of 2.2 to 4.0 Å (with a distribution having a peak at  $\sim 3.0$  Å, *SI Appendix, Fig. S7*). These results indicate that two salt-bridges interactions are possible, while one is strong, the other one is broken for a W-MT system. For W and M-MT systems, both the distances and corresponding distributions suggest the presence of both

salt-bridges simultaneously. Since classical dynamics may mislead the actual scenario due to poor sampling, we have carried out the 2D-free energy simulations using well-tempered metadynamics simulations to investigate the stabilities and conformation of the Arg203-Glu236 salt-bridge pair for the three systems (Fig. 4). Two densely populated regions are found in the free energy landscape for the W-MT system. The minimum at the region marked as A corresponds to a conformation where the salt-bridge involving the interaction between the NH1 and OE1 remains intact, but at the same time, the interaction between NH2 and OE2 is broken. The highlighted B region represents a symmetrically opposite conformation. For the W state, there are three minimum regions with comparable stability. In addition to minima A and B, there is a third minimum, marked as AB, which corresponds to the state having the two salt-bridges forming simultaneously. For the M-MT system, three similar minima are also present as observed for the W system but with the AB region being a more populated one. Therefore, MT binding to the wild-type kinesin stabilizes the broken conformation of the Arg203-Glu236 salt-bridge facilitating the pre-organization. On the other hand, Asn255Ser mutation secures the perfectly intact conformation of the Arg203-Glu236 salt-bridge pair disrupting the pre-organization.

**Mutation Perturbs the Optimal Geometry of Lytic Water.** Then, we turned our attention toward the lytic water. A water molecule is designated as a lytic water if the Ow1-P $\gamma$  distance is  $<4.5$  Å, the Ow1-H21 distance is  $<3.5$  Å, and the Ow1-P $\gamma$ -O $\beta$  angle is  $>100^\circ$  (Fig. 5 and *SI Appendix, Fig. S10*). A single

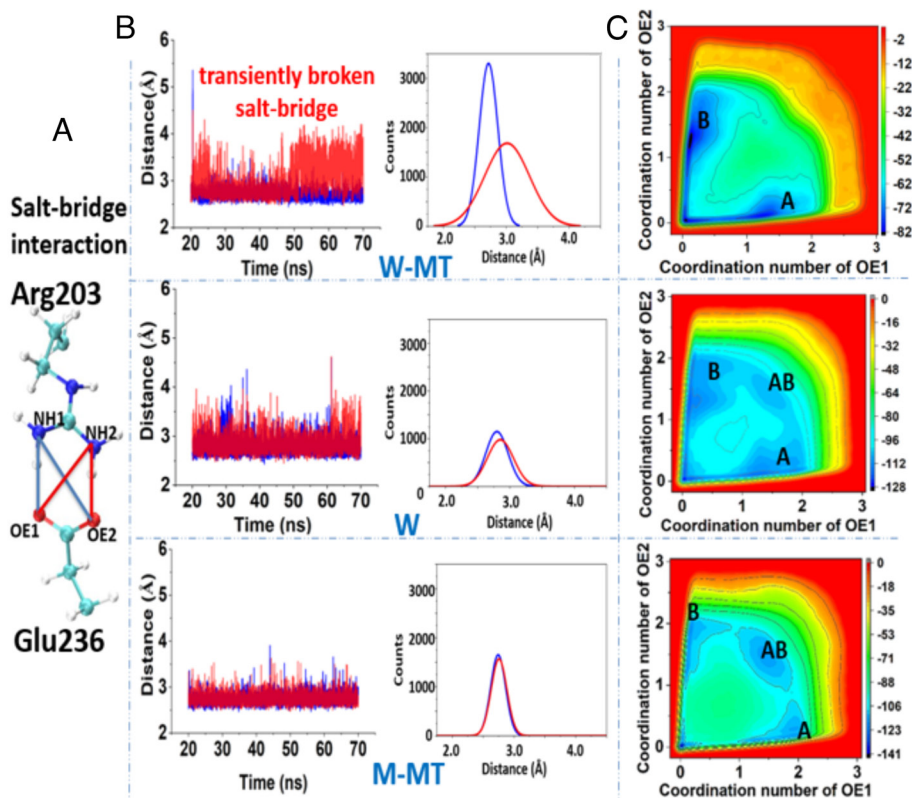


**Fig. 4.** The stability and orientation of the Arg203-Glu236 salt-bridge for three different systems (W-MT, W, and M-MT) using classical MD simulations. (A) The structure of the salt-bridge interactions between the Arg203 and Glu236 near the ATP-binding site of the kinesin motor. (B) The time evolution of the minimum distances of the NH1-OE1/OE2 (blue) and NH2-OE1/OE2 (red) obtained from classical MD simulations of three different systems. The distribution of these two distances, NH1-OE1/OE2 (blue) and NH2-OE1/OE2 (red), obtained from the classical MD simulations were also plotted. If the above-mentioned measured distance falls well below 3.5 Å, then it signifies a strong salt-bridge interaction between Arg203 and Glu236, while the distance toward 3.5 Å or above indicates the weak or broken salt-bridge. (C) The 2D-free energy profiles for the stability of the conformation states of the Arg203-Glu236 salt-bridge pair of the W-MT, W, and M-MT systems. The unit of free energy is kJ/mol.

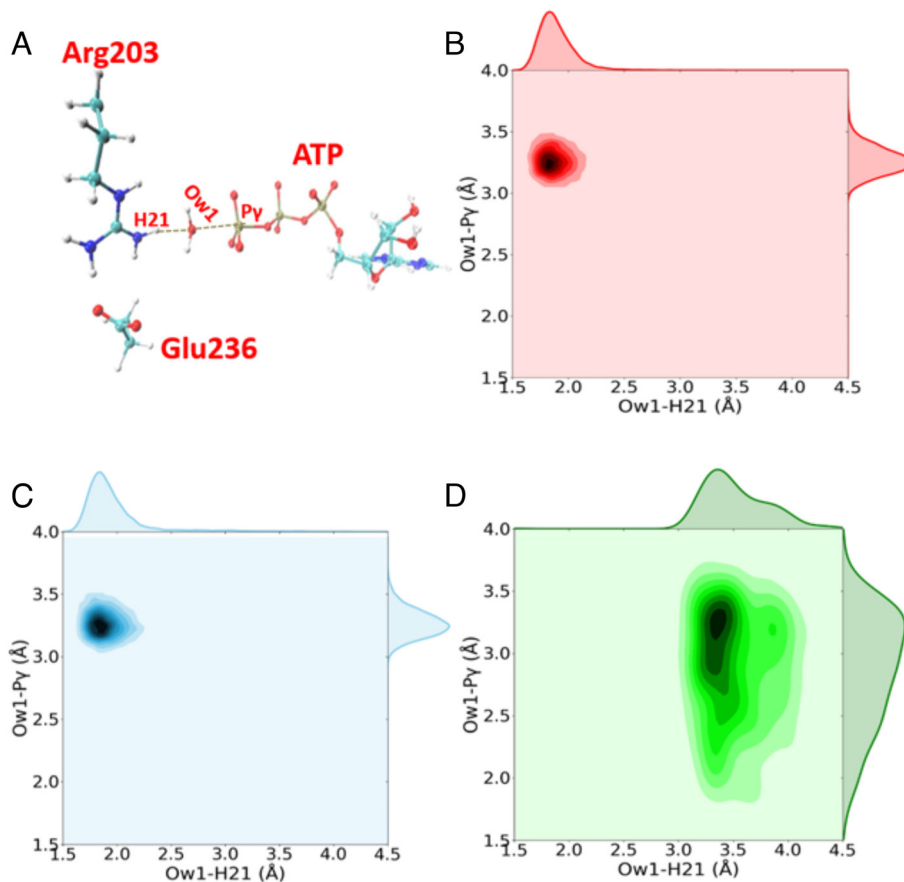


**Fig. 5.** The interactions of the lytic water with the side chain of Arg203. (A) The structure of broken Arg203-Glu236 salt-bridge, ATP molecule, and lytic water in the kinesin motor domain is displayed. The joint probability distribution plots of the interatomic distances of Ow1-H21 and Ow1-Py (in Å) are shown for the (B) W-MT, (C) W, and (D) M-MT systems.

lytic water molecule is present in all the frames throughout our simulation trajectories for the W and W-MT systems. On the contrary, the lytic water is detected in only ~10% of the total frames for the M-MT system (*SI Appendix, Fig. S11*). More importantly, while the identity of the lytic water does not change throughout the simulation for W and W-MT, it frequently changes its identity for the M-MT system. We observed that the lytic water molecule is slightly closer to the  $\gamma$ -phosphate of the ATP in the case of the W (Ow1-Py:  $3.27 \pm 0.01$  Å) and W-MT (Ow1-Py:  $3.27 \pm 0.02$  Å) systems than for the M-MT system (Ow1-Py:  $3.53 \pm 0.29$  Å). The angles of Ow-Py-O $\beta$  for the W-MT, W, and M-MT systems are  $154.5 \pm 5.5$ ,  $154.9 \pm 5.3$ , and  $130.2 \pm 21.1$  degrees. The ATP hydrolysis is generally an  $S_N2$ -type reaction for which the nucleophile (lytic water) should approach an electrophile at an angle of  $180^\circ$  with respect to the leaving group (O $\beta$ -ADP). Therefore, the angle distributions results suggest that the phosphate hydrolysis is more favorable for the W-MT and W systems than for the M-MT one (*SI Appendix, Fig. S10*). Interestingly, the lytic water forms a strong hydrogen bond between the oxygen atom of the lytic water and H21 atom of the Arg203 residue for the W system ( $1.97 \pm 0.03$  Å) and for the W-MT one ( $1.89 \pm 0.02$  Å) (Fig. 5). This hydrogen-bonding interaction helps to hold the lytic water in an optimum position for the hydrolysis reaction. This hydrogen-bonding interaction is weak and less frequently observed for the M-MT system ( $3.52 \pm 0.28$  Å) (Fig. 5). Additionally, we have calculated the number of water molecules forming a water chain between  $\gamma$ -phosphate of the

ATP and the Glu236 for these three systems (*SI Appendix, Figs. S8 and S9*).

#### Change in Local Environment Near the Mutation Site.

We explore the local environment near the mutation site (Asn255). We found that there are two stable hydrogen-bonding interactions. The  $\text{HN}_{\text{Glu236}}-\text{OD1}_{\text{Asn255}}$  (W:  $2.34 \pm 0.04$  Å and W-MT:  $2.35 \pm 0.05$  Å) and the  $\text{O}_{\text{Glu236}}-\text{HD22}_{\text{Asn255}}$  (W:  $2.24 \pm 0.04$  Å and W-MT:  $2.18 \pm 0.04$  Å) between the backbone of Glu236 and the side chain of the Asn255 residue for the W-MT and W systems (Fig. 6 and *SI Appendix, Figs. S12 and S13*). For the Asn255Ser mutation, the interatomic distances of  $\text{HN}_{\text{Glu236}}-\text{OG}_{\text{Ser255}}$  ( $5.93 \pm 0.07$  Å) and  $\text{O}_{\text{Glu236}}-\text{HG1}_{\text{Ser255}}$  ( $6.75 \pm 0.05$  Å) become quite large (*SI Appendix, Fig. S14*). Therefore, these two aforementioned hydrogen-bonding interactions are completely lost in the M-MT system (Fig. 6). Instead, a weak interaction is found between the HG1 atom of the side chain of Ser255 residue and the O atom of the backbone of the Met413 of  $\alpha$ -tubulin (*SI Appendix, Figs. S14 and S15*). This interaction makes the serine residue to rotate far away from the Glu236. Hence, a gap between the Ser255 and the Glu236 is created which allows more water molecules to flow into the ATP-binding site of the mutated M-MT system (Fig. 6).

Furthermore, multiple sequence alignment analysis of the different kinesin motors has demonstrated that the Agr203, Glu236, and Asn255 residues are highly conserved among different organisms (*SI Appendix, Fig. S16*). This finding suggests that those three residues have a crucial functional role in catalysis.

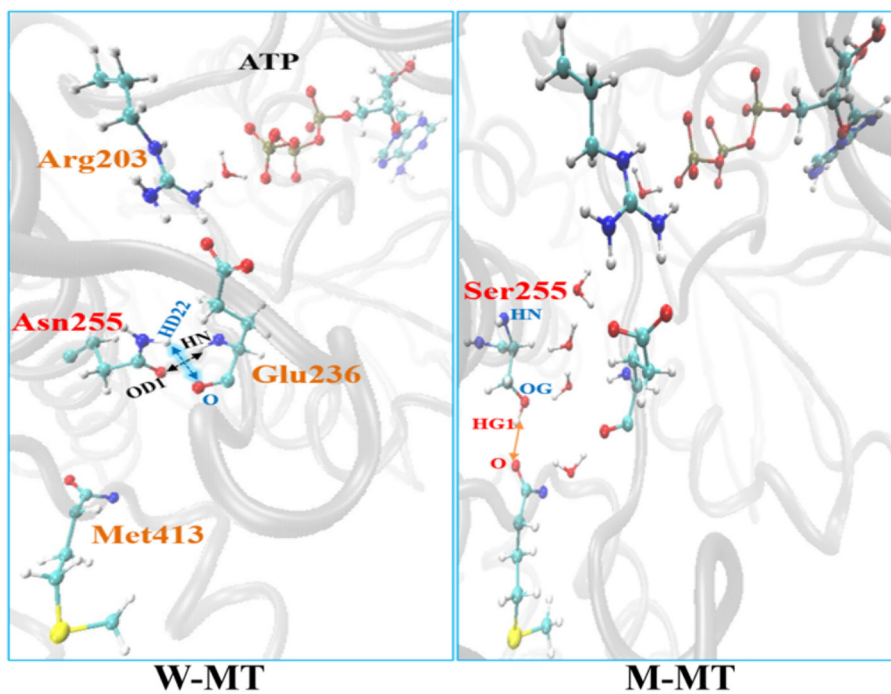


**Fig. 6.** The second sphere interactions network for the W-MT and M-MT systems. Snapshot structures highlighting the ATP, lytic water, Arg203-Glu236 salt-bridge, and Asn255 residue on kinesin motor domain region and Met413 residue on the  $\alpha$ -tubulin are shown for the W-MT, M-MT model systems.  $\text{HN}_{\text{Glu236}}-\text{OD1}_{\text{Asn255}}$  and  $\text{O}_{\text{Glu236}}-\text{HD2}_{\text{Asn255}}$  interactions for the W-MT and the  $\text{O}_{\text{Met413}}-\text{HG1}_{\text{Ser255}}$  interaction for the M-MT systems are displayed.

Taken together all the results obtained in our study, we can explain the modulation of the ATP hydrolysis rates observed in the experiments. Let's consider the rate constant of the ATP hydrolysis reaction for the optimal reorganized geometry as  $k_{\text{opt}}$ . Therefore, the observed rate of hydrolysis can be expressed as  $K_{\text{opt}}$  [Pre-organized] where [Pre-organized] is the concentration of optimal pre-organized geometry. Binding to MT [Pre-organized] of wild-type kinesin is found to be increased. This explains the few fold increase in ATP hydrolysis rate upon MT binding. On the contrary, the distal mutation of Asn255 residue decreases [Pre-organized] and thereby decreases the ATP hydrolysis rate.

## Conclusion

In conclusion, our analysis uncovered that the pre-organization environment of the ATP hydrolysis reaction of kinesin-1 is critically dependent on having the broken state of the Arg203-Glu236 salt-bridge sufficiently populated. This salt-bridge in turn is controlled by a second sphere Asn255 residue (also by MT-binding interactions located far away) through backbone-mediated interactions with Glu236. We demonstrated that the Asn255Ser mutation allosterically disrupts the whole interaction network, causing a destabilization of the pre-organization environment required for efficient ATP hydrolysis reaction in the kinesin motor. This disruption is responsible for the HSP disease in humans. In earlier studies, we have shown that some of the HSP-related genotypic mutations altered the energetic balance between the MT binding and coiled-coil dimerization interactions (8). Such a disruption affects the order-disorder transition of the neck linker domain leading to heavy loss in communication between the two motor head domains of the dimer. This makes kinesin very inefficient by reducing its processivity and therefore shortening of the MT run. In this work, we demonstrate that another genotypic mutation leads to impaired ATP hydrolysis by essentially making the kinesin

very sluggish on the MT. Such slow kinesin blocks the road ahead for other swiftly moving kinesins. The fate is again HSP disease. Therefore, different mutations in the same gene (genotypic mutation) manifest two distinct mechanisms in the phenotypic level but ultimately lead to the same HSP disease.

## Materials and Methods

**Setup of Enzyme Models and Classical MD Simulations.** The  $\alpha/\beta$ -tubulin-human kinesin 1-ADP- $\text{AlF}_4^-$  complex (PDB ID: 4HNA) was resolved by Gigant et al. (26) and used as an initial crystal structure for our present study. The  $\alpha/\beta$ -tubulins are heterodimers which are units of a MT. In this crystal structure, kinesin is bound with a stable ATP hydrolysis TS analogue, ADP- $\text{AlF}_4^-$ . To prepare our enzyme model system, the designed ankyrin repeat protein, which prevents tubulin self-assembly, is removed from the crystal structure. Then,  $\text{AlF}_4^-$  moiety of the ADP- $\text{AlF}_4^-$  is replaced with the  $\text{PO}_3$  group to prepare the ATP molecule. In the crystal structure, there was only one  $\text{Mg}^{2+}$  ion present in the ATP-binding site of the kinesin motor domain region and two crystallographic water molecules were also present that are bound with the  $\text{Mg}^{2+}$  ion. The three model systems have been prepared in this present investigation, for instance, wild-type- $\alpha/\beta$ -tubulin complex (W-MT), Asn255Ser-mutated- $\alpha/\beta$ -tubulin complex (M-MT), and wild-type kinesin (W). In the case of a mutated (M-MT) system, the asparagine residue in the 255th residue of the kinesin motor domain was mutated with the serine residue. The classical MD simulations have been performed to equilibrate the ATP-bound enzyme complexes using Gromacs 5.1 simulations program (27). The atomic charges and force field parameters of the ATP molecule were obtained by SwissParam (28), a topology builder compatible with CHARMM forcefield (29). The Charmm 27 force field parameters (30) were used for the entire protein. The ATP-enzyme complexes were subsequently solvated in a cubic box with a 10 Å radius layer of water molecules using the TIP3P water model (31). Then, the entire ATP-bound enzyme complex was neutralized by adding 37 sodium ions for the W-MT and M-MT model systems, and six sodium ions for the W model system. Afterwards, the resulting systems of the W, W-MT, and M-MT were energy minimized with 50,000 steps of steepest descent method. The long-range cutoff for nonbonded interactions was taken as 10 Å for all the above minimization steps and also for all subsequent MD simulations. The electrostatic interactions are treated using particle mesh Ewald method (32). We apply the LINCS algorithm to constrain bonds

involving hydrogen atoms (33). The minimum image convention and the periodic boundary conditions were applied in all directions. A time step of 1 fs is used in all MD simulations. The Berendsen barostat and the Berendsen thermostat (34) were used to control the pressure and temperature with relaxation times of 1 ps and 0.1 ps, respectively. The system was simulated at 300 K for 250 ps using the NVT ensemble, and 70 ns of MD simulation is performed using NPT ensemble for each system. Visual MD (VMD) 1.9.2 is used in order to study trajectories and explore atomic-level insights (35). GROMACS 5.1 toolkit has been employed to further analysis of each system.

**Metadynamics Simulations for the 2D-Free Energy Calculations.** The well-tempered metadynamics (36) simulations were performed in order to compute the two-dimensional free energy profiles for the stability of the Arg203-Glu236 salt-bridge pair using the PLUMED 2.4.3 plugin (37) for GROMACS. Combination of metadynamics and collective variables (CVs) techniques has shown to be a successful treatment for complex systems. In the Arg203-Glu236 salt-bridge pair, the OE1 and OE2 atoms of the carboxylic moiety of the Glu236 interact with the hydrogen atoms of the NH1 and NH2 atoms of the Arg203. (Fig. 1 and Fig. 4) The effective way to measure the stability of the Arg203-Glu236 salt-bridge is to determine the coordination numbers of OE1 and OE2 atoms. We have used the coordination number as effective CVs for our 2D-free profiles calculations. The coordination number calculates the number of contacts between two groups of atoms which represents a distance-dependent switching function ( $s_{ij}$ ).

$$s_{ij} = \frac{1 - \left(\frac{r_{ij}-d_0}{r_0}\right)^n}{1 - \left(\frac{r_{ij}-d_0}{r_0}\right)^m}$$

In this 2D-free energy profile, first group along the X-axis displays coordination of the OE1 atom of the Glu236 with four hydrogen atoms of the NH1 and NH2 moieties of the Arg203 residue. The second group along the Y-axis describes the coordination linkage of the OE2 atom with the aforementioned four hydrogen atoms of Arg203, respectively. This switching function ( $s_{ij}$ ) is close to one, if  $r_{ij} \leq r_0$ , otherwise, the function smoothly decays to zero, when  $r_{ij} > r_0$ . On the other hand, the values of  $r_0$ ,  $d_0$ ,  $m$ , and  $n$  used in the metadynamics simulations are 0.25 nm, 0, 12, and 6, respectively. The bias factor, height, and width of the added Gaussian were 15, 0.25 kJ/mol, and 0.05, respectively, and hills were deposited in every 10 steps.

**QM/MM Calculations.** QM/MM optimization calculations were carried out using configurations of ATP-bound kinesin-tubulin complex derived from our classical MD simulations. For the ATP hydrolysis reaction, three models (designated as models A, B, and C, respectively) were constructed (Fig. 2). All three models have the same number of QM atoms (106). The QM region is comprised of the side chains of the Glu236, Arg203, Ser202, and Thr92 residues, as well as the  $Mg^{2+}$  ion, ATP, and six water molecules. The valence of the QM subsystem was saturated by adding four-link atoms between the  $C_\gamma$  and  $C_\beta$  atoms of the Glu236, Arg203, Ser202, and Thr92 residues. The remaining protein, water atoms, and 37  $Na^+$  ions are located in the MM area. We applied OPLS-AA (38) and TIP3P potentials to enzymes and water, respectively. The B3LYP functional and Pople's 6-31+G(d,p) basis set for all atoms were used to describe the QM region (39, 40). The micro-macro-iteration approach implemented by the f-DYNAMO package (41) and its interface with Gaussian 09, (42) which was successfully used to probe various enzymatic reactions, were used to perform the QM/MM calculations (43–45). The existence of a distinct imaginary frequency expressing the appropriate reaction coordinate was used to validate the TS structures. Then, single-point calculations employing dispersion-included B3LYP-D3/def2-TZVP/OPLS level of theory were used to correct the energies of all the optimized stationary state structures (46–49).

**Data, Materials, and Software Availability.** All study data are included in the article and/or *SI Appendix*.

**ACKNOWLEDGMENTS.** R.N.M. is thankful to Indian Association for the Cultivation of Science and SERB, DST, PDF/2017/00324 for providing fellowship. This research is partly supported by the Department of Science and Technology (DST) SERB grant CRG/2020/000756. J.N.O. is supported by the National Science Foundation (NSF) grants PHY-2019745 and PHY-2210291) and by the Welch Foundation (Grant C-1792). J.N.O. is a Cancer Prevention and Research Institute of Texas (CPRI) Scholar in Cancer Research. We also thank Dr. Mandira Dutta, Dr. Sridip Parui, and Souvik Dey for helpful discussions.

Author affiliations: <sup>a</sup>School of Chemical Sciences, Indian Association for the Cultivation of Science, Kolkata 700032, India; <sup>b</sup>Center for Theoretical Biological Physics, Rice University, Houston, TX 77005; <sup>c</sup>Department of Physics and Astronomy, Rice University, Houston, TX 77005; <sup>d</sup>Department of Chemistry, Rice University, Houston, TX 77005; and <sup>e</sup>Department of Biosciences, Rice University, Houston, TX 77005

- G. Woehlke, M. Schliwa, Walking on two heads: The many talents of kinesin. *Nat. Rev. Mol. Cell Biol.* **1**, 50–58 (2000).
- N. Hirokawa, Y. Noda, Y. Tanaka, S. Niwa, Kinesin superfamily motor proteins and intracellular transport. *Nat. Rev. Mol. Cell Biol.* **10**, 682–696 (2009).
- H. T. Vu, Z. Zhang, R. Tehver, D. Thirumalai, Plus and minus ends of microtubules respond asymmetrically to kinesin binding by a long-range directionally driven allosteric mechanism. *Sci. Adv.* **8**, eabn0856 (2022).
- N. Hirokawa, R. Takemura, Molecular motors in neuronal development, intracellular transport and diseases. *Curr. Opin. Neurobiol.* **14**, 564–573 (2004).
- M. L. Giudice *et al.*, A missense mutation in the coiled-coil domain of the KIF5A gene and late-onset hereditary spastic paraplegia. *Arch. Neurol.* **63**, 284–287 (2006).
- S. Jennings *et al.*, Characterization of kinesin switch I mutations that cause hereditary spastic paraplegia. *PLoS One* **12**, e0180353 (2017).
- B. Ebbing *et al.*, Effect of spastic paraplegia mutations in KIF5A kinesin on transport activity. *Hum. Mol. Genet.* **17**, 1245–1252 (2008).
- M. Dutta, M. R. Diehl, J. N. Onuchic, B. Jana, Structural consequences of hereditary spastic paraplegia disease-related mutations in kinesin. *Proc. Natl. Acad. Sci. U.S.A.* **115**, E10822–E10829 (2018).
- M. Dutta, S. P. Gilbert, J. N. Onuchic, B. Jana, Mechanistic basis of propofol-induced disruption of kinesin processivity. *Proc. Natl. Acad. Sci. U.S.A.* **118**, e2023659118 (2021).
- C. Hyeon, J. N. Onuchic, A structural perspective on the dynamics of kinesin motors. *Biophys. J.* **101**, 2749–2759 (2011).
- R. Takaki, M. L. Mugnai, Y. Goldtzvik, D. Thirumalai, How kinesin waits for ATP affects the nucleotide and load dependence of the stepping kinetics. *Proc. Natl. Acad. Sci. U.S.A.* **116**, 23091–23099 (2019).
- Z. Zhang, Y. Goldtzvik, D. Thirumalai, Parsing the roles of neck-linker docking and tethered head diffusion in the stepping dynamics of kinesin. *Proc. Natl. Acad. Sci. U.S.A.* **114**, E9838–E9845 (2017).
- E. M. Craig, H. Linke, Mechanochemical model for myosin V. *Proc. Natl. Acad. Sci. U.S.A.* **106**, 18261–18266 (2009).
- J. Czub, M. Wiczór, B. Prokopowicz, H. Grubmüller, Mechanochemical energy transduction during the main rotary step in the synthesis cycle of F1-ATPase. *J. Am. Chem. Soc.* **139**, 4025–4034 (2017).
- M. L. Mugnai, D. Thirumalai, Step-wise hydration of magnesium by four water molecules precedes phosphate release in A Myosin motor. *J. Phys. Chem. B* **125**, 1107–1117 (2021).
- M. Dutta, B. Jana, Exploring the mechanochemical cycle of dynein motor proteins: Structural evidence of crucial intermediates. *Phys. Chem. Chem. Phys.* **22**, 33085–33093 (2016).
- D. Mondal, A. Warshel, EF-Tu and EF-G are activated by allosteric effects. *Proc. Natl. Acad. Sci. U.S.A.* **115**, 3386–3391 (2018).
- F. A. Kiani, S. Fischer, Comparing the catalytic strategy of ATP hydrolysis in biomolecular motors. *Phys. Chem. Chem. Phys.* **18**, 20219–20233 (2016).
- R. N. Manna, M. Dutta, B. Jana, Mechanistic study of the ATP hydrolysis reaction in dynein motor protein. *Phys. Chem. Chem. Phys.* **22**, 1534–1542 (2020).
- S. Hayashi *et al.*, Molecular mechanism of ATP hydrolysis in F1-ATPase revealed by molecular simulations and single-molecule observations. *J. Am. Chem. Soc.* **134**, 8447–8454 (2012).
- N. Vithani, S. Batra, B. Prakash, N. N. Nair, Elucidating the GTP hydrolysis mechanism in FeoB: A hydrophobic amino-acid substituted GTPases. *ACS Catal.* **7**, 902–906 (2017).
- A. R. Calixto *et al.*, GTP Hydrolysis without an active site base: A unifying mechanism for ras and related GTPases. *J. Am. Chem. Soc.* **141**, 10684–10701 (2019).
- M. J. McGrath, I.-F. W. Kuo, I.-F. W. Hayashi, S. Takada, ATP hydrolysis mechanism in kinesin studied by combined quantum mechanical / molecular-mechanical metadynamics simulations. *J. Am. Chem. Soc.* **135**, 8908–8919 (2013).
- B. L. Grigorenko, A. V. Rogov, I. A. Topol, S. K. Burt, H. M. Martinez, Mechanism of the myosin catalyzed hydrolysis of ATP as rationalized by molecular modelling. *Proc. Natl. Acad. Sci. U.S.A.* **104**, 7057–7061 (2007).
- X. Lu, V. Ovchinnikov, D. Demapan, D. Roston, Q. Cui, Regulation and plasticity of catalysis in enzymes: Insights from analysis of mechanochemical coupling in Myosin. *Biochemistry* **56**, 1482–1497 (2017).
- B. Gigant *et al.*, Structure of a kinesin-tubulin complex and implications for kinesin motility. *Nat. Struct. Mol. Biol.* **20**, 1001–1007 (2013).
- M. J. Abraham *et al.*, GROMACS: High performance molecular simulations through multi-level parallelism from laptops to supercomputers. *Software X* **1–2**, 19–25 (2015).
- V. Zoete, M. A. Cuendet, A. Grosdidier, O. Michielin, SwissParam: A fast force field generation tool for small organic molecules. *J. Comput. Chem.* **32**, 2359–2368 (2011).
- B. R. Brooks *et al.*, CHARMM: A program for macromolecular energy, minimization, and dynamics calculations. *J. Comput. Chem.* **4**, 187–217 (1983).
- K. Zinovjev, E. Liepinsh, Validation of the CHARMM27 force field for nucleic acids using 2D nuclear overhauser effect spectroscopy. *J. Biophys. Chem.* **4**, 58 (2013).
- P. Mark, L. Nilsson, Structure and dynamics of the TIP3P, SPC, and SPC/E water models at 298 K. *J. Phys. Chem. A* **105**, 9954–9960 (2001).
- T. Darden, D. York, L. Pedersen, Particle mesh Ewald: An N-Log(N) method for Ewald sums in large systems. *J. Chem. Phys.* **98**, 10089–10092 (1993).



33. B. Hess, H. Bekker, H. J. Berendsen, J. G. Fraaije, LINCS: A linear constraint solver for molecular simulations. *J. Comput. Chem.* **18**, 1463–1472 (1997).
34. H. J. Berendsen, J. V. Postma, W. F. van Gunsteren, A. R. H. J. DiNola, J. R. Haak, Molecular dynamics with coupling to an external bath. *J. Chem. Phys.* **81**, 3684–3690 (1984).
35. W. Humphrey, A. Dalke, K. Schulten, VMD: Visual molecular dynamics. *J. Mol. Graph.* **14**, 33–38 (1996).
36. A. Barducci, G. Bussi, M. Parrinello, Well-tempered metadynamics: A smoothly converging and tunable free-energy method. *Phys. Rev. Lett.* **100**, 020603 (2008).
37. M. Bonomi *et al.*, PLUMED: A portable plugin for free-energy calculations with molecular dynamics. *Comput. Phys. Commun.* **180**, 1961–1972 (2009).
38. W. L. Jorgensen, J. Tirado-Rives, The OPLS [optimized potentials for liquid simulations] potential functions for proteins, energy minimizations for crystals of cyclic peptides and crambin. *J. Am. Chem. Soc.* **110**, 1657–1666 (1988).
39. C. Lee, W. Yang, R. G. Parr, Development of the colle-salvetti correlation-energy formula into a functional of the electron density. *Phys. Rev. B Condens. Matter* **37**, 785–789 (1988).
40. R. Krishnan *et al.*, A basis set for correlated wave function. *J. Chem. Phys.* **72**, 650–654 (1980).
41. M. J. Field, M. Albe, C. Bret, F. Proust-De Martin, A. Thomas, The dynamo library for molecular simulations using hybrid quantum mechanical and molecular mechanical potentials. *J. Comput. Chem.* **21**, 1088–1100 (2000).
42. M. J. Frisch *et al.*, Gaussian 09, Revision A.02 (Gaussian, Inc., Wallingford CT, 2016).
43. K. Swiderek, I. Tuñón, I. H. Williams, V. Moliner, Insights on the origin of catalysis on glycine N-methyltransferase from computational modeling. *J. Am. Chem. Soc.* **140**, 4327–4334 (2018).
44. R. García-Meseguer, S. Martí, J. J. Ruiz-Pernía, V. Moliner, I. Tuñón, Studying the role of protein dynamics in an SN2 enzyme reaction using free-energy surfaces and solvent coordinates. *Nat. Chem.* **5**, 566–571 (2013).
45. R. N. Manna, T. Malakar, B. Jana, A. Paul, Unraveling the crucial role of single active water molecule in the oxidative cleavage of aliphatic C-C bond of 2,4'-dihydroxyacetophenone catalyzed by 2,4'-dihydroxyacetophenone dioxygenase enzyme: A quantum mechanics/molecular mechanics investigation. *ACS Catal.* **8**, 10043–10050 (2018).
46. S. Grimme, S. Ehrlich, L. Goerigk, Effect of the damping function in dispersion corrected density functional theory. *J. Comput. Chem.* **32**, 1456–1465 (2011).
47. S. Grimme, J. Antony, S. Ehrlich, S. A. Krieg, Consistent and accurate ab initio parametrization of density functional dispersion correction (DFT-D) for the 94 elements H-Pu. *J. Chem. Phys.* **132**, 154104 (2010).
48. F. Weigend, R. Ahlrichs, Balanced basis sets of split valence, triple zeta valence and quadruple zeta valence quality for H to Rn: Design and assessment of accuracy. *Phys. Chem. Chem. Phys.* **7**, 3297–3305 (2005).
49. F. Weigend, Accurate Coulomb-fitting Basis Sets for H to Rn. *Phys. Chem. Chem. Phys.* **8**, 1057–1065 (2006).